



Article

Relationship between TIR and NIR-SWIR as Indicator of Vegetation Water Availability

Mauro Ezequiel Holzman ^{1,*}, Raúl Eduardo Rivas ² and Martín Ignacio Bayala ²

¹ Consejo Nacional de Investigaciones Científicas y Técnicas, Instituto de Hidrología de Llanuras “Dr. Eduardo Jorge Usunoff” (IHLLA), Rep. Italia 780, Azul B7300, Argentina

² Comisión de Investigaciones Científicas de la Provincia de Buenos Aires, Instituto de Hidrología de Llanuras “Dr. Eduardo Jorge Usunoff” (IHLLA), Tandil B7000, Argentina; rivas@rec.unicen.edu.ar (R.E.R.); mbayala@ihlla.org.ar (M.I.B.)

* Correspondence: m.holzman@ihlla.org.ar

Abstract: Water availability for vegetation use has been associated with the relative amount of water in the plant and is a key factor for modeling variables related to the soil-plant system (e.g., net primary production, drought effects on vegetation). To the best of our knowledge, the integration of spectral proxies of vegetation water content (near-infrared (NIR), shortwave-infrared (SWIR) bands) and land surface temperature (LST) for estimation, not only of vegetation water content but also soil water available for the evapotranspiration process requires more analysis. This study aims to assess the relationship between NIR, SWIR reflectance, and LST data as indicators of water availability for crop use. For this purpose, vegetation water content, LST, and spectral reflectance over soybean, corn, and barley were measured in the field and the laboratory. Based on the consistency of satellite data from Moderate-Resolution Imaging Spectroradiometer (MODIS/Aqua) in relation to such measurements, a model is proposed, which can be parameterized from remotely sensed NIR-SWIR/LST scatterplots. The obtained results were tested in the Argentine Pampas, showing coherence with surface processes at regional scale associated with soil water availability. The comparison with soil moisture at different depths ($R^2 > 0.7$) showed that the method is sensitive to variations in root zone water availability. Given the reliance of the index on just satellite data, it can be pointed that the potential not only for vegetation water stress analyses but also in the context of hydrological modeling as an input of water availability.

Keywords: energy balance; water vegetation status; optical/thermal; drought



Citation: Holzman, M.E.; Rivas, R.E.; Bayala, M.I. Relationship between TIR and NIR-SWIR as Indicator of Vegetation Water Availability. *Remote Sens.* **2021**, *13*, 3371. <https://doi.org/10.3390/rs13173371>

Academic Editor: Hongtao Duan

Received: 21 June 2021

Accepted: 19 August 2021

Published: 25 August 2021

Publisher's Note: MDPI stays neutral with regard to jurisdictional claims in published maps and institutional affiliations.



Copyright: © 2021 by the authors. Licensee MDPI, Basel, Switzerland. This article is an open access article distributed under the terms and conditions of the Creative Commons Attribution (CC BY) license (<https://creativecommons.org/licenses/by/4.0/>).

1. Introduction

Water availability for vegetation use is a key variable for modeling net primary production, drought effects on vegetation, and susceptibility to fire due to its association with transpiration, photosynthesis, vegetation stress, and flammability [1]. Vegetation water scarcity affects physiological processes that determine vegetation growth; thus, it has been widely studied in agricultural lands and terrestrial ecosystems [2,3]. Vegetation water status has been commonly associated with water stress. Typical field methods for vegetation water status measurement include pressure chambers, thermocouple psychrometers, leaf porometers that measure stomatal conductance, and destructive field sampling that considers the weight of water in the leaves, among others [4,5]. However, these methods are difficult to integrate at a landscape or regional scale, given the spatial changes in soil moisture and atmospheric conditions (e.g., incoming solar radiation, evaporative demand). In this sense, remote sensing techniques have contributed to the estimation of vegetation water content over large areas.

Over the last few decades, various remote sensing approaches have been investigated to monitor vegetation water content. Commonly, they consider visible, near-infrared (VIS-NIR, 0.3–1.0 μm), short-wave infrared (SWIR, 1.0–2.5 μm), and mid-wave infrared (MIR,

2.5–6.0 μm) reflectance data [2,5–8]. VIS and NIR have been frequently used to obtain vegetation indices showing changes in photosynthetic activity, given the interaction of solar radiation with leaf pigments in VIS and the high reflectance of healthy vegetation in NIR. However, these indices show changes due to re-arrangement of the cellular space and leaf structure after a long stress process, which has also been reported at the canopy level [5,6].

Other parts of the solar spectrum, like SWIR wavebands, have been widely associated with early biophysical symptoms of water stress like leaf water content and stomatal conductance due to the strong absorption of liquid water at those wavelengths [7–11]. The estimation of the vegetation water content has been frequently analyzed with NIR and SWIR data with the purpose of studying vegetation water stress [4]. Incident solar radiation in the SWIR bands is absorbed by liquid water with no influence of foliar pigment absorption; thus, the reflectance of canopies has been associated with liquid water in the leaves [5,11]. Common SWIR wavebands show a strong correlation with leaf water content range between 1.6 μm and 2.5 μm [9,12,13]. Several authors stated that NIR is less effective for estimating this variable, given the lower sensitivity to changes in leaf water content, compared with the SWIR [14,15]. Model simulations have shown a high sensitivity at 0.86 μm to changing water content, which explains the frequent use of this band as a reference for formulating indices sensitive to water content [4]. However, leaf structure and dry matter content could influence the SWIR reflectance. Given that NIR is mainly affected by dry matter [16], by subtracting NIR and SWIR, these effects can be removed, improving the estimation of water content [17,18] (Figure 1). Ref. [4] shows an interesting review of optical methods for the estimation of leaf water content from remotely sensed data.

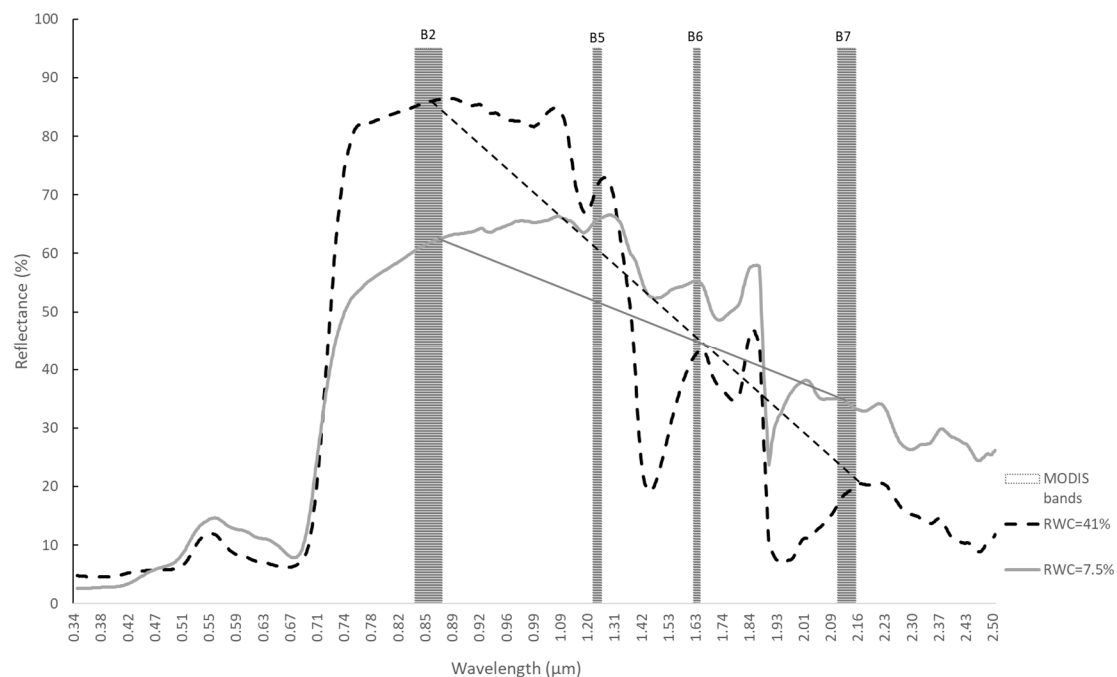


Figure 1. Spectral reflectance measured in the laboratory using spectrometer SVC HR-1024i from soybean leaves with two different values of relative water content. Straight lines show the difference between NIR and SWIR reflectances (in this case, bands centered at 0.86 and 2.13 μm , respectively), which rise with increasing leaf water content. As an example, bands of MODIS sensor in NIR and SWIR (bands 2, 5, 6, and 7) are included.

Previous studies have shown a strong relationship between vegetation water content and narrow-band indices based on NIR-SWIR domains [5,14,17,19–21]. Ref. [18] reported low redundancy between the normalized difference vegetation index (NDVI) and an index based on NIR (band 2 of MODIS, 0.841–0.876 μm) and SWIR (band 6 of MODIS, 1.628–1.652 μm) during the vegetative phase in Senegal. Ref. [14] showed that the SWIR is

sensitive to changes in leaf water content on different eucalyptus species, with the highest correlation coefficient approximately between 1.6–1.8 μm and 2.1–2.2 μm .

The study of water stress using only spectral data seems to be complex, given the existence of simultaneous processes. A large obstacle when estimating vegetation water content from reflectance data at the landscape level is the effect of LAI, soil, and background, given its spatial and temporal changes [4]. On the other hand, [22] stated that in drying soils, changes in root metabolism could produce a decrease in growth and stomatal conductance, reducing evapotranspiration. Ref. [23] suggested that water stress induces photochemical changes as soon as stomata close, but leaf water content decreases when soil moisture reaches a certain threshold. Moreover, the rate of transpiration depends mainly on the supply of water to the evaporating surfaces, the supply of energy to vaporize water, and the resistances in the vapor pathway [22]. Thus, changes in stomatal aperture are affected not only by internal factors like pressure and relative water content but also by environmental variables with complex interactions between them.

Plants need to maintain a continuous flux of water to preserve vital processes such as photosynthesis and nutrient uptake. Drought conditions for a plant are mainly determined by soil moisture availability, which controls the plant water potential and hence cell turgor and water content. After the cooling effect of transpiration has been reduced by the presence of water deficit, heat or radiation stress frequently appears [24]. Given that surface temperature largely depends on soil moisture, Thermal Infrared (TIR, 8–14 μm) has been widely used to detect signs of water stress [25]. Land Surface Temperature (LST expressed in K) is an indicator of energy balance at canopy level, specifically the relation between latent (evapotranspiration) and sensible heat fluxes [25–27], according to the simplified surface energy balance equation:

$$R_n = LE + H + G \quad (1)$$

where R_n is the net radiation, LE is the latent heat flux (evapotranspiration or ET), H is the sensible heat flux (heat transferred due to the difference between LST and air temperature), and G is the soil heat flux (which is almost negligible under maximum vegetation cover) (all are expressed in W m^{-2}). Over vegetated areas, the distribution of incoming solar radiation into H and LE depends strongly on stomatal resistance to transpiration and root zone soil moisture (all atmospheric forcing and surface roughness being equal) [28,29]. Stomatal resistance is crucial because water escapes mainly from plants through open stomata—the more energy for evapotranspiration, the less sensible heating of the surface (low LST). Thus, LST is an indicator of H ($\approx R_n - LE$) and evapotranspiration [25,27].

A few works have analyzed the relationship between vegetation water content and thermal data. Some of them suggested a better response in the solar domain than that provided by thermal information. However, some points should be discussed. Ref. [30] reported a more noticeable spectral response of three plant species in the MIR than in the TIR. With the integration of different spectrometers measurements, some works investigated the entire spectral range (i.e., VIS to TIR) to retrieve leaf water content. Ref. [13] found a high coefficient of determination in MIR and SWIR with poorer results in TIR over eleven plant species. However, such a relationship is not straightforward, given that fluctuations in leaf internal structure, cuticle thickness, and surface characteristics can produce changes in reflectance unrelated to water content [14,31]. Ref. [31] studied the effect of water and temperature stress on two plant species (European beech and rhododendron), analyzing TIR spectra and the leaf emissivity derived from a spectrometer (Bruker Vertex 70 FTIR). They reported significant changes after water stress, showing variations according to water content and cuticle thickness. However, it should be noted that changes in TIR spectra are significantly less than in the solar domain, with the consequent possible reflectance fluctuations due to different sources of noise not related to water content (e.g., changes in measurement/observational conditions).

Given that leaf temperature is sensitive to changes in resistance to the process of sensible heat flux, it can be a complementary indicator to vegetation water status indices

as a proxy of root zone soil moisture available for vegetation use. Also, one of the main advantages of thermal data is the high sensitivity to short-time vegetation water stress. LST has been frequently associated with surface soil moisture given the relation with thermal inertia, although, in over vegetated areas, it is strongly influenced by root zone soil moisture according to the cooling process due to evapotranspiration [26,28]. Ref. [32] used SWIR and LST in a downscaling algorithm to provide soil moisture maps at a higher resolution than the original one of Soil Moisture Ocean Salinity (SMOS). They found good agreement between such indices and surface soil moisture (0–5 cm depth) in Spain. Refs. [33,34] reported that the SWIR waveband includes the optimal bands in the solar domain for remote sensing of surface soil moisture. They suggested a model based on a linear relationship between soil moisture and NDVI/SWIR reflectance instead of the well-known NDVI/LST model. They assumed a linear relationship between root zone soil moisture and leaf water content, but the validation was carried out at 0–5 cm depth. To the best of our knowledge, the integration of spectral proxies of vegetation water content and LST to develop a model, not only for vegetation water content estimation but also soil water available for evapotranspiration with minimum requirements of ancillary measurements requires more analysis.

In this context, the aim of this study is to evaluate the relationship between NIR-SWIR reflectance and LST and their ability as indicators of water availability for vegetation use. Thus, the contribution to the study of the effect of water stress on plants is expected. Specifically, such a relationship is tested with in situ measurements of spectra, LST, vegetation water content, subsurface soil moisture, and medium-resolution remote sensing images.

2. Materials and Methods

2.1. Study Area

The Argentine Pampas is one of the most productive plains in the world, covering more than 50 million hectares for crop production and livestock. As only about 10% of agricultural lands are irrigated, water availability is a common limiting factor for grain production, especially for summer crops (mainly soybeans and corn). Field measurements were carried out in three test sites with physical characteristics and agricultural practices representative of the study area: Tandil station (37°19' S, 59°05' W), La Campana (37°17' S, 58°56' W) and La Ydalina (35°09' S, 61°07' W) (Figure 2). Tandil station and La Campana are located in Northern Hills, an agro-climatic region characterized by a sub-humid temperate climate, mean annual rainfall about 950 mm, reference evapotranspiration of 1000 mm, with usual water excess during autumn and winter and occasional water deficit in summer [29]. Typic Argiudoll is the dominant soil type, with silty loam texture in the A horizon and silty clay loam in deep horizons, high organic matter content (3–5%) in superficial horizons, and high water retention capacity (\approx 170–220 mm at 0.8 m depth). Wheat and barley are the main winter crops, soybeans and corn are dominant in summer.

In Sandy Pampas, the mean annual precipitation is about 800 mm showing an east–west gradient, and is slightly lower than reference evapotranspiration, with short periods of water deficits in summer [25]. Entic Hapludoll with sandy loam texture is the dominant soil, with lower water retention capacity (\approx 90–130 mm at 0.8 m depth) than Northern Hills. Soybeans and corn are the main summer crops. It should be noted that crop yield in the study area is highly dependent on water availability, and important fluctuations have been reported in the last years due to water scarcity [25,29].

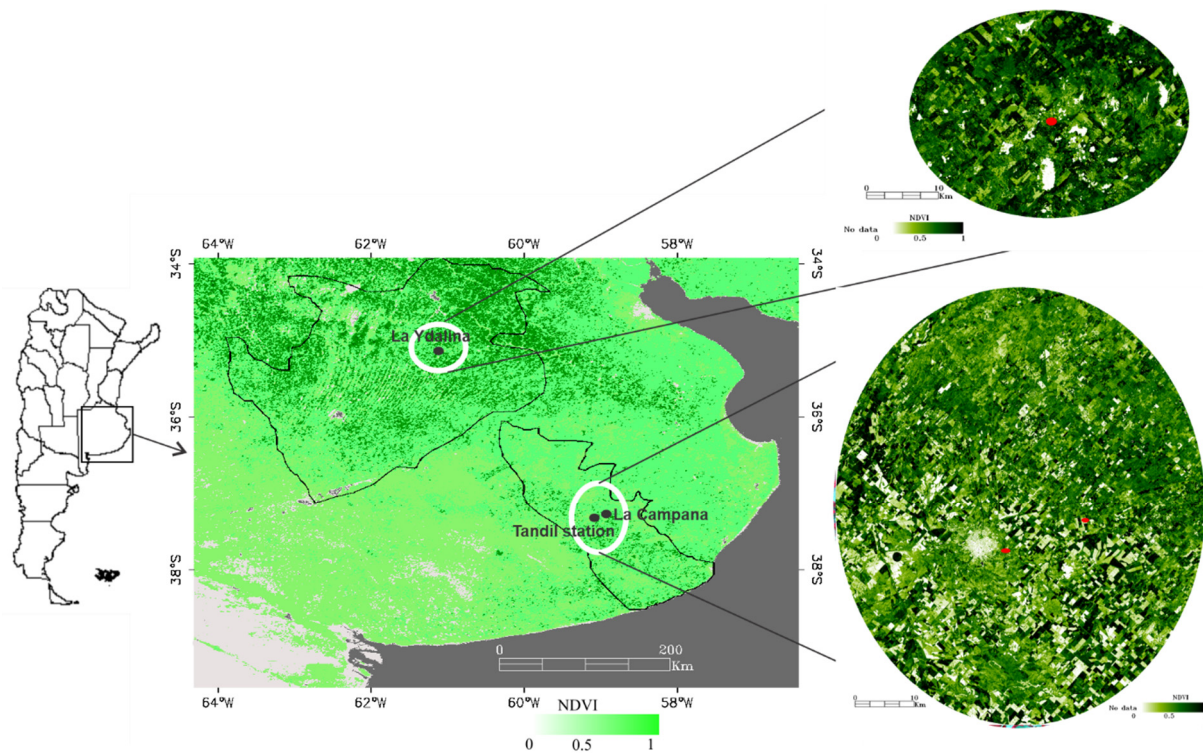


Figure 2. Location of the Argentine Pampas and the three test sites where field measurements were carried out (red circles). (left) maps of NDVI from MODIS/Aqua, (right) NDVI from Landsat 8 (date: 2 January 2019).

2.2. Field Data

2.2.1. Leaf and Canopy Spectral/Thermal Measurements

Spectral reflectance measurements over soybean, corn, and barley were taken between 0.35 and 2.50 μm with the spectrometer SVC HR-1024i (Spectra Vista Corporation, USA), $\text{FOV} = 4^\circ$. This spectrometer can acquire spectra with a sampling interval of $\leq 0.0033 \mu\text{m}$, 0.7 μm ; $\leq 0.0095 \mu\text{m}$, 1.5 μm ; $\leq 0.0065 \mu\text{m}$, 2.1 μm . A reference reflectance spectralon panel (99%) was used to convert raw incident radiance to spectral reflectance [35]. All spectral measurements were made in a nadir orientation of the spectrometer, with a distance of about 0.4 m between the spectrometer and the canopy. Spectra were recorded under two conditions: (1) laboratory, on the collected soybean leaves post hydration and during the progressive dehydration process, (2) field, every 15 m of each transect. In the laboratory, the 5–7 collected leaves per plant were arranged horizontally, taking spectra on the adaxial surface. In La Campana station, 2 plots of soybeans and 1 of corn were selected for measuring reflectance along transects during dates of full vegetation cover and different hydric conditions (15 February 2019 and 28 February 2019). Also, 1 plot of barley was monitored during November 2019 to test the behavior of a winter crop. Sampling locations were selected so that canopy conditions were fairly homogeneous in surrounding areas at scales of 10 m. Measurements were taken under cloud-free conditions diurnally between 10:30 and 16:00 local time. The studied crops are representative of the regional ones, and the dates were selected to study the sensitivity of spectral/thermal data to changes in vegetation water availability over the same cover.

Foliage temperatures were measured immediately after obtaining spectra with an ST PRO Raytek (8–14 μm), which has a resolution of 0.1 $^\circ\text{C}$ and accuracy of about 0.3 $^\circ\text{C}$ for the typical range of temperature. LST was obtained by hand-holding the thermometer directly over each plant (or group of leaves in the case of the laboratory) and looking down at the leaves from about 0.5 m above the canopy with an angle of about 70° from horizontal, which always allowed full-plant cover. We assumed an emissivity of 0.98 for all cases.

2.2.2. Vegetation Water Content

At each stop along transects where spectra were recorded, foliar samples were collected by cutting the plants of barley and 5–7 leaves of soybean at the top of the canopy. They were immediately weighed using a portable electronic balance with an accuracy of 0.01 g (model ES-1200HA, Jadever Scale Co., Xiamen, China) to obtain the fresh mass (Fw). After weighing, leaves were placed in sealed plastic bags and transported to the laboratory. In the laboratory, samples were hydrated with distilled water to determine leaf mass at 100% water content (Tw). Afterward, they were exposed to the sun, dried at ambient temperature, and then oven-dried at 50 °C until dry weights were constant to obtain dry mass (Dw). The Fw was determined during the dehydration process, previous to each reflectance measurement. These weights were used to obtain gravimetric estimations of relative water content (RWC, %):

$$\text{RWC} = \frac{Fw - Dw}{Tw - Dw} \times 100 \quad (2)$$

The RWC compares the actual leaf water content with the maximum water content at full turgor. It is a common water content index in plant physiology to determine plant water status [17].

2.2.3. Soil Moisture

Soil moisture is a key factor controlling plant water potential and then cell turgor and RWC. To test the sensitivity of NIR-SWIR/LST data to root zone soil moisture, a comparison with field measurements was carried out. On La Ydalina station (35°09' S, 61°07' W), a tensiometer connected to a Davis Vantage Pro2 (Davis Instruments Corporation) station was used to measure soil moisture at 60- and 120-cm depths. Values at 5-cm depth were also considered, although it is expected that they have significant fluctuations, especially in sandy soils and that plants extract water from deeper soil horizons. Relative soil water content (%) was determined from tension measurements (in centibars) by the moisture-characteristic curve previously defined in the laboratory. On Tandil station (37°19' S, 59°05' W), the sensors EC-10 H2O and EC-20 H2O (Decagon Devices, Inc., USA) measured water content (%) at 10-, 40-, and 60-cm depths. Both probes measured the integrated dielectric constant (in millivolts) at 10- and 20-cm depths, respectively, which is related to the volumetric water content. With the sole purpose of showing the behavior of NIR-SWIR and LST on bare soil with different surface water content, measurements were taken with a Delta-T ThetaProbe ML2x soil moisture probe. The sensors were calibrated for each soil type [36,37]. Finally, from NIR-SWIR/LST images obtained from MODIS/Aqua, daily values for a kernel of 3 × 3 in size were compared with soil moisture data. This comparison was carried out for January–March 2012, when simultaneous data in Tandil and La Ydalina stations were available.

2.3. Relationship between NIR-SWIR/LST in 2D Space from Satellite Data

In this study, a narrow band normalized difference index as a traditional indicator of leaf water content (e.g., [18,19]) was calculated using the reflectance of MODIS sensor band 2 (0.841–0.876 μm) and band 7 (2.105–2.155 μm):

$$\text{NIR} - \text{SWIR}_{\text{index}} = \frac{\rho_{\text{NIR}} - \rho_{\text{SWIR}}}{\rho_{\text{NIR}} + \rho_{\text{SWIR}}} \quad (3)$$

where ρ_{NIR} and ρ_{SWIR} are the daily surface reflectance of bands 2 and 7 of the MODIS sensor, respectively. We named the index as a generalized equation based on the normalized difference between NIR and SWIR, given that several previous works have defined different indices according to different wavebands. As shown in Figure 1, the index will take high values in the case of a spectrum with SWIR reflectance lower than NIR reflectance, showing high vegetation water content.

Following the concepts discussed in the Introduction, a conceptual model of the complementation between remotely sensed data of LST and NIR-SWIR can be proposed in Figure 3 (left), which shows a scatterplot for the study area that includes heterogeneous hydric conditions. The index is based on the difference of reflectance between NIR and SWIR increases with the leaf water content and also with increasing vegetation cover [38]. However, moderate water stress frequently does not produce vegetation water content changes since the plant tries to maintain a level compatible with its basic functioning, reducing transpiration [39]. Thus, LST could be a complement of a NIR-SWIR index given that minimum water availability reduces ET and increases H (sensible heat flux changes can be assessed by surface temperature LST). In a scatterplot for a study area that includes heterogeneous hydric conditions and vegetation cover (from full cover to bare soil), an edge of minimum water availability for plant use, and surface soil moisture in the case of bare soil, is expected to be a quadratic adjustment. Such an edge of minimum ET indicates maximum water stress. The quadratic function would be more consistent with biophysical processes of the soil-plant system than a linear edge of the approaches based on LST and vegetation indices, given that the intercept value of linear adjustment is difficult to find in natural conditions. Conversely, the linear edge of maximum ET (minimum LST) represents high soil water availability for plants and the conduction of heat from the soil-plant system into the atmosphere. These edges can fluctuate depending on climatic conditions (e.g., atmospheric water demand, dry/wet periods), whereby such changes should be considered if large regions with different atmospheric forces are being analyzed. It should be noted that this shape of the scatterplot would not depend on the spatial resolution if the mentioned heterogeneous surface conditions are included.

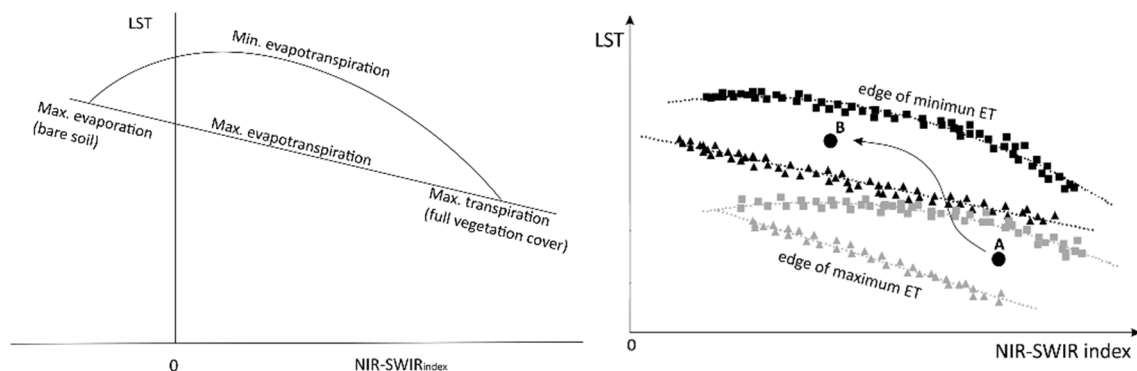


Figure 3. (left) general conceptual model of the NIR-SWIR/LST relationship (see $\text{NIR} - \text{SWIR}_{\text{index}}$ in Equation (3)). (right) Interpretation of remotely sensed LST/NIR-SWIR scatterplot using two examples of daily MODIS/Aqua data for the study area ($\text{EVI} > 0.3$). Triangles (rectangles) indicate edges of maximum (minimum) evapotranspiration (ET), and hence, water availability in the soil-plant system. The TIDI for a given pixel (e.g., A or B) is based on the distance to the edges. A path from A to B is suggested as a drying process for a given pixel. Grey: edges for a widespread wet condition, black: edges for a dry condition.

Soil reflectance varies with soil type, particle size distribution, bulk density of the soil, and organic matter content, but also strongly with surface water content [34]. Our measurements over bare soils indicate that the $\text{NIR-SWIR}_{\text{index}}$ assumes negative values, although previous studies reported slightly positive ones for saturated soils (e.g., [40,41]). On bare soils, LST is mainly related to surface soil moisture, associated with thermal inertia and evaporative control. Under conditions of high atmospheric evaporative demand and incoming solar radiation (e.g., during summer), low LST reflects high surface water content and maximum evaporation from bare soil.

Figure 3 (right) shows a remotely sensed LST/NIR-SWIR scatterplot from daily MODIS/Aqua data for the study area that includes heterogeneous hydric conditions, partially and fully vegetated surfaces. These vegetated areas were selected considering an Enhanced Vegetation Index (EVI) higher than 0.3; this vegetation index is similar to

the NDVI but takes into account the canopy background and atmospheric scattering with improved sensitivity into high biomass regions. A hypothetical path of a drying pixel (from point A to B) is proposed. It should be noted that this path is not straightforward and depends on the temporal response of LST and NIR-SWIR according to leaf water content and energy balance. These aspects can be analyzed more deeply in future studies. Nevertheless, to obtain information on water availability for vegetation use from remotely sensed data at a regional scale, an index called TIDI (Temperature-Infrared Dryness Index) is proposed:

$$\text{TIDI} = \frac{\text{LST} - \text{LST}_{\min}}{\text{LST}_{\max} - \text{LST}_{\min}} = \frac{\text{LST} - a_1(\text{NIR} - \text{SWIR}_{\text{index}}) + b_1}{\left[a_2(\text{NIR} - \text{SWIR}_{\text{index}})^2 + b_2(\text{NIR} - \text{SWIR}_{\text{index}}) + c_2 \right] - (a_1(\text{NIR} - \text{SWIR}_{\text{index}}) + b_1)} \quad (4)$$

where LST is the observed surface temperature at a given pixel, LST_{\min} is the minimum LST in the LST/NIR-SWIR scatterplot (the linear edge reflecting maximum actual ET), LST_{\max} is the quadratic edge of maximum LST in the LST/NIR-SWIR scatterplot representing minimum actual ET and, hence, water availability. $\text{NIR-SWIR}_{\text{index}}$ is an index based on the difference between surface reflectance in NIR and SWIR bands (see Equation (4)). The parameters a_1 , a_2 , b_1 , b_2 , and c_2 of the edges are characteristic of each image and can vary depending on hydric conditions (Figure 3). The edges can be determined using least square quadratic and linear regression for LST_{\max} and LST_{\min} , respectively, from daily to 16/days scatterplots, depending on the objectives of the study. This index takes values between 0 near the LST_{\min} (maximum water availability) and 1 for pixels near LST_{\max} (minimum water availability).

For a good estimation of the TIDI parameters, certain points should be taken into account. The study area should include dry and wet soils (minimum soil water content and near field capacity), which would represent minimum evapotranspiration (LST_{\max}) and potential evapotranspiration (LST_{\min}), respectively. Uniform atmospheric conditions in the study area are preferable to avoid low sensitivity due to extreme conditions in the same dataset (e.g., desert and humid areas). Also, seasonal fluctuations mainly produced by atmospheric changes (e.g., incoming solar radiation, atmospheric water demand) can be expected. In this sense, extreme edges (minimum LST_{\min} and maximum LST_{\max}) can be defined for the study period to avoid such temporal fluctuations of the parameters. Thus, the calculation of TIDI is normalized using the same parameters. On the other hand, the index is recommended for monitoring vegetation water stress over large agricultural lands; the sensitivity over native vegetation should be tested in future studies. Also, water bodies or irrigated surfaces in the study area could be considered to test the LST_{\min} as an indicator of maximum or potential evapotranspiration [28].

Horizontal variation of surface (e.g., LST differences between vegetation and bare soil) or atmospheric conditions can produce large-scale advection. This process is more noticeable under extreme conditions as irrigated crops in arid or semi-arid areas, producing variations in evapotranspiration from surrounded areas to the crop. Other cases of heterogeneous landscapes can include land and water bodies or topography variations. This aspect should be considered when evaluating the evapotranspiration from crops growing under these conditions. Although more local studies should be done to evaluate the advection, the spatial resolution of current thermal missions can monitor changes in heat fluxes at synoptic or mesoscale.

In this study, two Moderate Resolution Imaging Spectroradiometer (MODIS) products were considered for TIDI calculation: (1) MYD11A1: daily MODIS/Aqua LST (K) at 1-km resolution, which includes atmospherically corrected per-pixel temperature and emissivity values, and (2) MYD09GA: daily MODIS/Aqua surface reflectance at 500-m resolution, which provides surface spectral reflectance corrected of atmospheric scattering and absorption for bands 1 to 7. Both products include cloud-free images; thus, cloudy pixels with value = 0 were masked out. Aqua satellite covers the hours of maximum atmospheric demand, so these data were used to analyze the influence of water availability

on TIDI. Also, the analyzed months (January, February, and November) cover the period of full vegetation cover of summer and winter crops, respectively, minimizing the bare soil signal.

LST and reflectance data were reprojected into geographic latitude/longitude coordinates, Datum WGS-84 with the MODIS Conversion toolkit. LST product was resampled to 500-m resolution to match up the MYD09GA resolution [42]. Then, 2 images for each day were mosaicked to cover the entire study area. After that, daily 2-D scatterplots of LST in function of the NIR-SWIR_{index} were analyzed to obtain daily values of the TIDI. It should be noted that a, b, and c parameters of LST_{max} and LST_{min} are characteristic of each image, varying mainly in the function of hydric conditions in the study area (see Figure 3). Daily scatterplots during the study period were analyzed to define the extreme edges and standardize the study series of the index. The extreme LST_{min} (linear adjustment with the lowest intercept and slope) would represent maximum evapotranspiration if the study period includes wet periods. The extreme LST_{max} (highest quadratic equation in the scatterplot) indicates the driest condition over the study period.

Figure 4 includes a summary of the applied method.

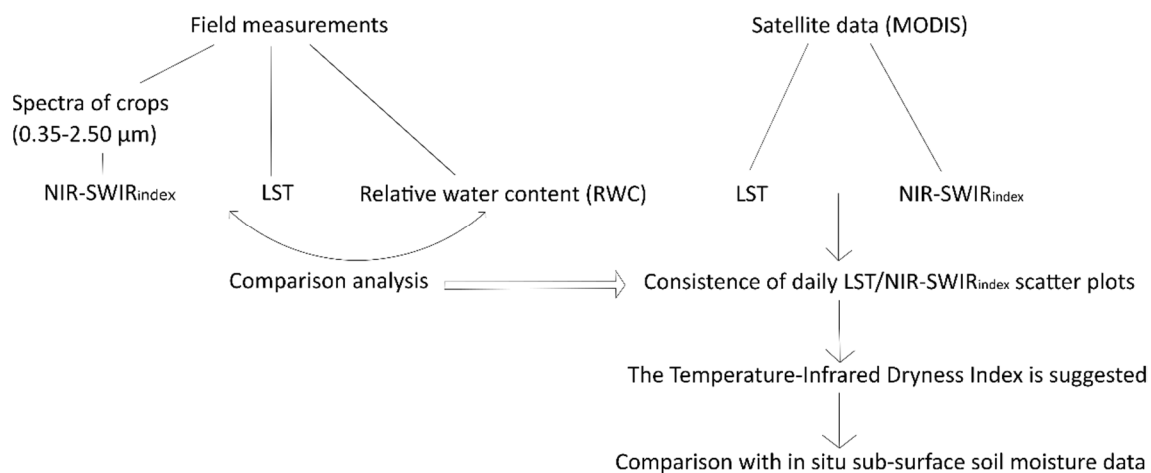


Figure 4. Flowchart of the applied method using in situ and satellite data.

3. Results and Discussion

3.1. Relationship between NIR-SWIR, LST and Leaf Water Content at Field Scale

Reflectance spectra of leaves obtained in the laboratory during the dehydration process indicate that the combination of NIR and SWIR reflects changes in leaf water content (Figure 5). The spectra show high reflectance in NIR, especially for high leaf water content, while SWIR reflectance increases due to decreasing amounts of leaf water. These results are consistent with several previous studies that showed strong absorption of liquid water in SWIR (e.g., [5,43]). High and intermediate RWC (60% and 44%) showed similar reflectance, around 1.6 μm . Conversely, the highest differences in SWIR were observed approximately at a wavelength higher than 2 μm . This wavelength includes atmospheric windows where the absorption by water vapor in the atmosphere is low. Also, it should be noted that the quality of band 6 of MODIS is not optimal because of noisy detectors [44]. Considering these points, bands 2 and 7 were used to compute the TIDI.

The reflectance index obtained in the laboratory during the dehydration process for samples of soybean and barley leaves showed a positive correlation with RWC, as reported in several previous studies (e.g., [8–10], among others) (Figure 6). Also, a positive correlation was observed considering wavelengths around 1.650 ($R^2 = 0.7$). However, a low correlation was observed between LST and RWC, showing that LST are not directly related to leaf water content. Commonly, when the turgor pressure decreases because of water deficit, the partly closed stomata results in a reduction in transpiration and hence the movement of water from the soil to leaves. In general, moderate or short-time water

stress frequently does not produce significant changes in leaf water content since the plant tries to maintain a certain level compatible with physiological processes, reducing transpiration [39]. This behavior should be more noticeable in isohydric crops, which can constantly regulate the water loss within a certain range to avoid damage due to water deficit. On the other hand, in anisohydric crops (e.g., soybeans and barley), the stomatal response to fluctuations in water potential is reduced, and they can maintain photosynthetic capacity during moderate stress. However, under more intense water stress, increases in LST should be a clear sign of water deficit. Also, it should be noted that the differences between these two types of crops are frequently difficult to note at a regional scale. Thus, the combination of NIR-SWIR data as a proxy of leaf water content and LST indicator of evapotranspiration can contribute to the monitoring of interdependent processes associated with the effects of water scarcity on vegetation.

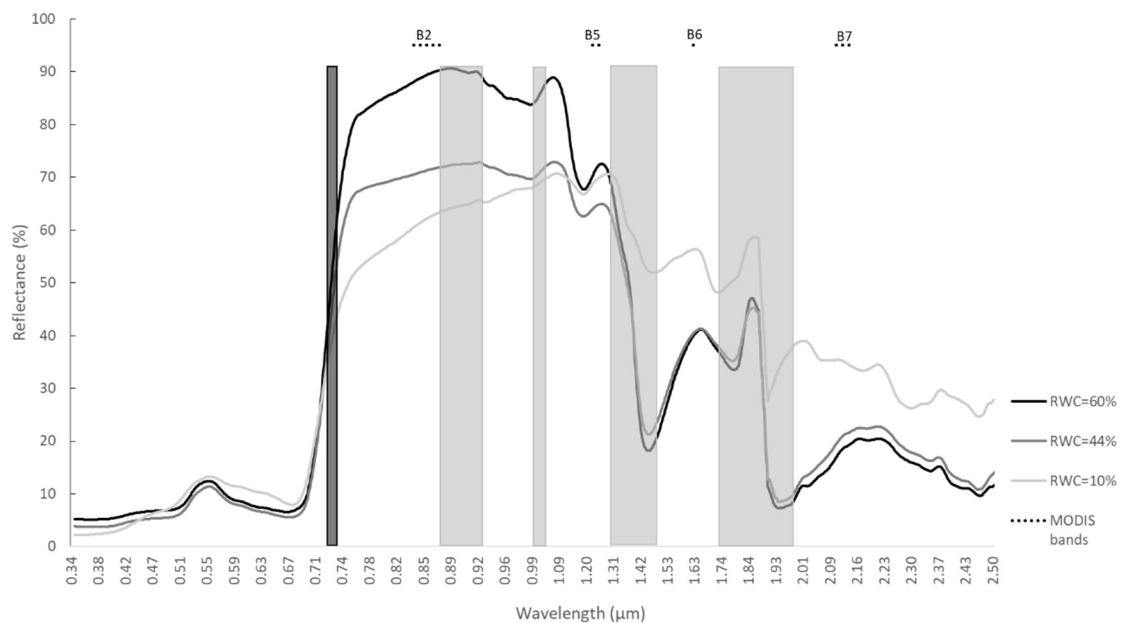


Figure 5. Reflectance spectra for soybean leaves with different water content. The intervals of strong atmospheric water vapor (grey rectangles), MODIS bands, and oxygen absorption (black rectangle) are included.

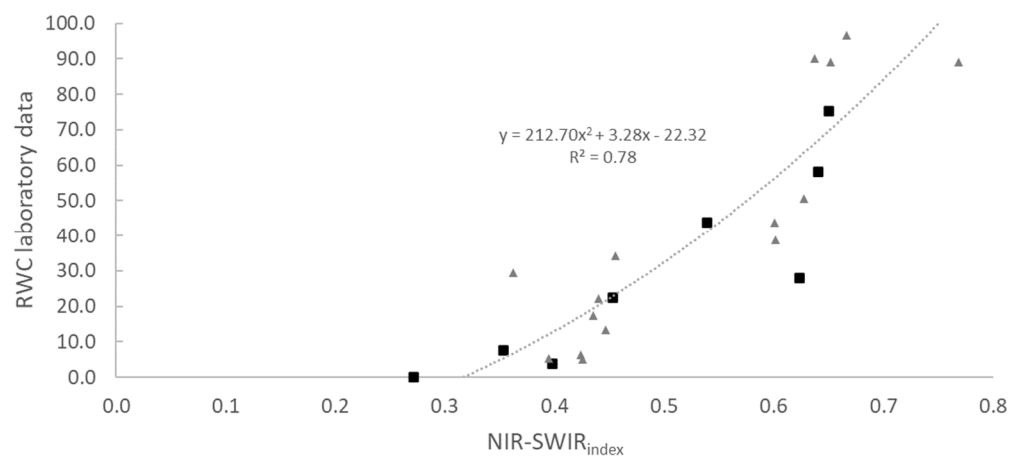


Figure 6. Relationship between leaf water content (RWC) and NIR-SWIR_{index} during the dehydration process of soybean (rectangles) and barley (triangles) samples.

Field measurements of LST and spectra were consistent with the general interpretation of the NIR-SWIR/LST relationship proposed in Figure 3 (Figure 7). In Figure 7, data from MODIS/Aqua for a subset (approximately 68,600 km², January–February 2019) are

included to contextualize the field measurements. Water deficit produced significant increases of LST for different NIR-SWIR_{index} values, describing a behavior similar to a quadratic function for maximum LST. Corn showed a slight trend to high LST values more frequently than soybean and barley, given that corn is more susceptible to water stress. Also, the limiting effect of low soil moisture increases as atmospheric conditions favor high potential rates of transpiration. Corn leaf rolling, a clear sign of water stress, was observed in the field where the highest LST were measured. Although a lag between transpiration and water absorption can produce symptoms of water stress in leaves exposed to the sun during midday of hot summer days, such leaf rolling was observed throughout the whole days of lowest water availability. Signs of wet conditions were more frequently observed in barley, given that it is a winter crop and there is less atmospheric evaporative demand during winter and spring.

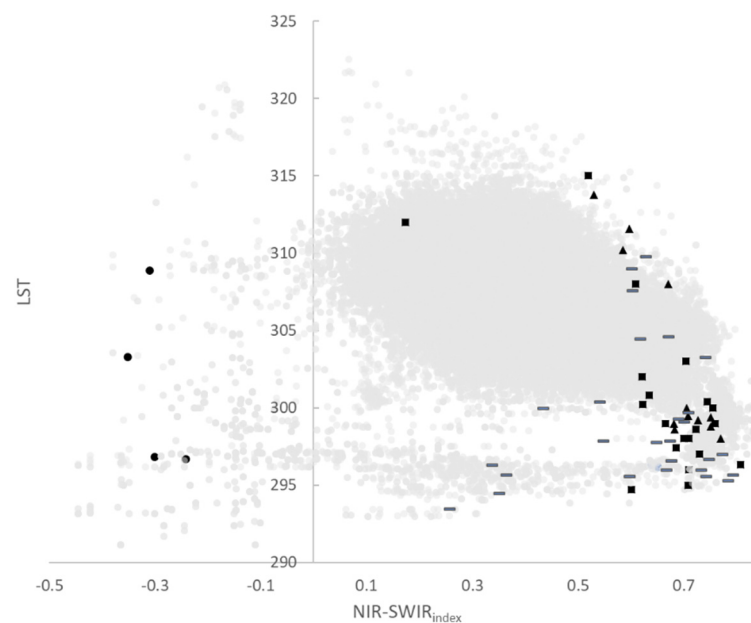


Figure 7. LST (K)/NIR-SWIR_{index} scatterplot of field measurements taken during three campaigns of different water availability for crops use (triangles: corn; rectangles: soybean; lines: barley; circles: bare soil). Daily remotely sensed data from MODIS/Aqua of the study area for days with different hydric conditions are included (light grey color).

On the other hand, surface soil moisture measurements over bare soil took negative values of NIR-SWIR_{index} with minimum LST for near-saturated soils. It should be noted that measurements were taken over Typic Argiudoll. Changes in reflectance can be expected in other soil types, depending on different factors such as bulk density, organic matter content, mineral composition. This point has been reported in previous studies such as [34] that showed changes in spectral reflectance of different soils for various levels of surface volumetric water content.

3.2. Parameters and Spatial Variability of TIDI

Daily LST/NIR-SWIR_{index} scatterplots during January and mid-March 2012 show the existence of high variability of water availability for vegetation use (Figure 8). These dates cover the main growth stages of summer crops in the study area. Although the classification of crop types was not carried out, the study area is a vast surface of flatlands containing quite homogeneous rain-fed croplands, with corn and soybeans being the dominant summer crops. Given that the study is focused on vegetation, bare soil and low vegetation cover were omitted in the scatterplots with a mask for $EVI \leq 0.3$. Thus, the lower linear edge with a negative slope and the quadratic upper limit were better defined. Observations were consistent with the proposed conceptual model, decreasing LST with the

increases of NIR-SWIR_{index}. Flat scatterplots characterized by low slope and intercept were expected under regional humid conditions, mostly due to the generalized cooling of the surface. These low maximum LST were observed on certain dates as 26 January–2 February and 16 March (monthly rainfall around 50 mm greater than the historical average for 120 years). A predominance of positive NIR-SWIR_{index} values suggesting wet conditions was noticeable mainly on 16 March. On 3 January, positive values were also evident, but the slope of LST_{min} and the pattern of LST_{max} suggested that the thermal data gave complementary information to optical ones. Although a wide range of NIR-SWIR_{index} was evident, LST showed higher variability, reflecting more sensitivity to short-time fluctuations of hydric conditions.

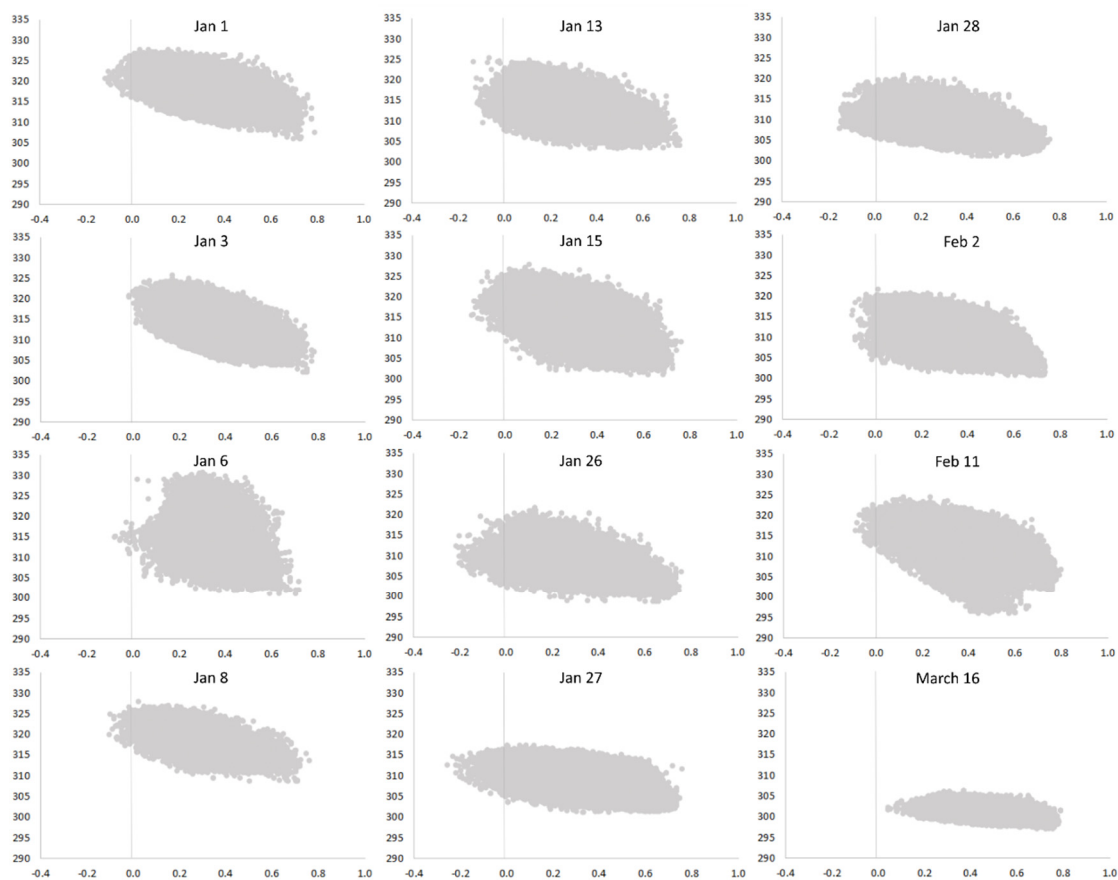


Figure 8. Examples of daily scatterplots of LST (K) (y -axis) and NIR-SWIR_{index} (x -axis) from MODIS/Aqua measurements for vegetated surfaces in the study area during January and mid-March 2012.

As mentioned previously (Section 2.3), the TIDI parameters are characteristic of each image, so the minimum LST_{min} and maximum LST_{max} of the study period were defined to compute daily TIDI: $LST_{max} = -27.3(NIR - SWIR_{index})^2 + 0.09(NIR - SWIR_{index}) + 329.3$; $LST_{min} = -24.6(NIR - SWIR_{index}) + 303.7$. It should be noted that a large area (68,600 km²) was considered in the scatterplots to include a wide range of water availability; otherwise, homogeneous hydric conditions would produce a poor estimation of these parameters. Also, the calculated edges reflect the expected regional maximum and minimum water availability for vegetation use during the study period.

Daily maps of TIDI show high spatial variability of water availability for vegetation (Figure 9). The general pattern is consistent with changes in topography, groundwater, and oceanic influence [45,46]. Thus, wet areas are located on the east and north-east edge due to the oceanic and shallow groundwater table influences. The water deficit was more evident westward, consistent with a semi-arid climate and sandy soils [28]. Dry areas were observed during early January, especially on 1 January. This water deficit is crucial for summer crops,

given the occurrence of critical growth stages during January and February, which largely determine crop yield [25]. On 1 January, water scarcity was noticeable westward in the semi-arid Pampas, especially in the upper areas of east-west valleys characterized by sandy soils with low water retention capacity, which favors moisture-stressed areas.

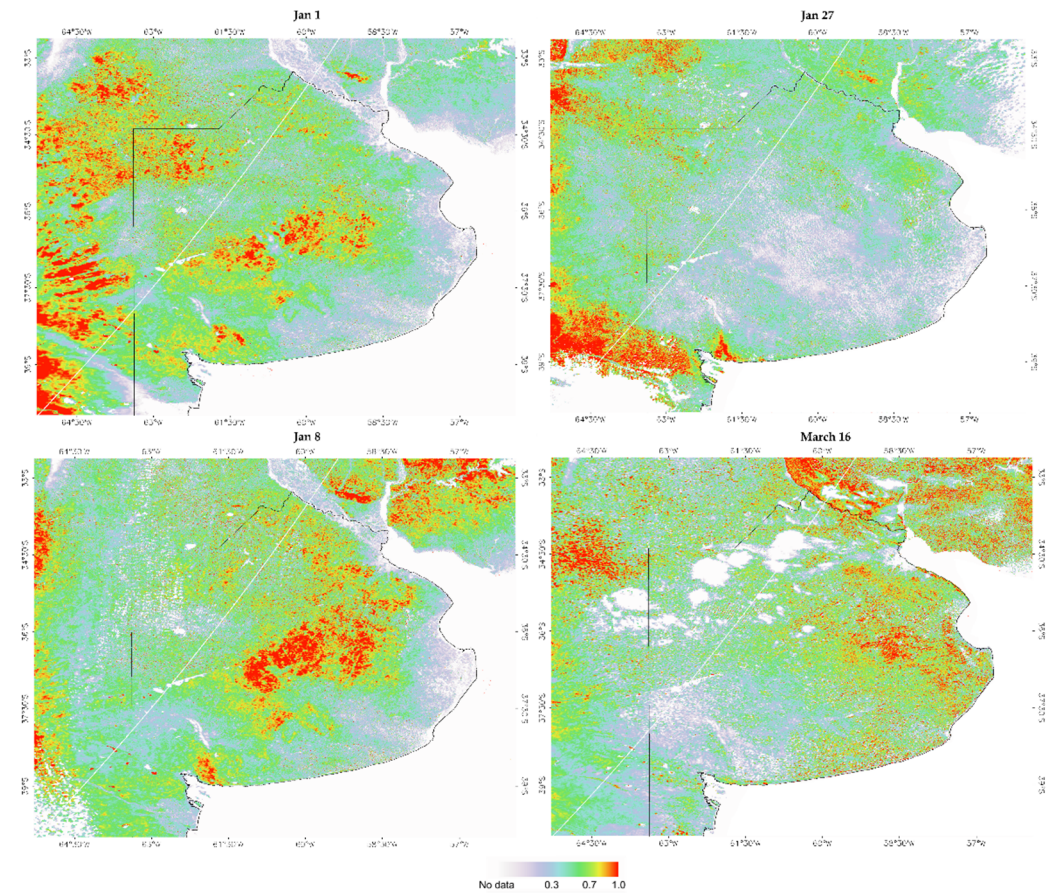


Figure 9. Examples of daily maps of TIDI at 500 m spatial resolution, without data for cloud cover and water bodies.

It should be noted that the spatial pattern of TIDI is expected to be related not only to atmospheric and vegetation cover variables (e.g., rainfall, atmospheric water demand, solar radiation, phenological phases) but also to subsurface soil moisture. Thus, in rapid drying soils, the spatial variability of TIDI would be more related to deep than surface soil moisture, which could be associated with different factors like water retention capacity of the soil, shallow groundwater table and capillarity effect or physical limitation to water movement (e.g., horizon with low hydraulic conductivity).

At this point, diverse positive characteristics related to the applicability of the TIDI can be highlighted. One is its suitability for hydrological and water stress vegetation studies with limited data availability, given the dependence on satellite data. Its calculation from satellite missions with frequent overpasses can provide near real-time estimation of water availability over large areas. However, some points should be taken into account for a good performance of the TIDI. Given the assumption that water availability is the main factor affecting the index, the study area should be reasonably uniform in atmospheric conditions, incoming solar radiation, and aerodynamics properties. On the other hand, despite its simple parameterization, the study area should be sufficiently heterogeneous to include a wide range of soil moisture. In this manner, the empirical LST_{min} and LST_{max} obtained from NIR-SWIR_{index} scatterplots are almost equal to the theoretical edges (potential evapotranspiration and minimum evapotranspiration, respectively), avoiding an overestimation (underestimation) of LST_{min} (LST_{max}) in case of a predominance of dry (wet) conditions.

The influence of cloud cover on surface reflectance and LST should be considered if a continuous calculation of the index is needed, not only due to the lack of data but also the effect of cloud shadows (e.g., Figure 9, 16 March). In this study, cloudy areas and cloud shadows were masked. In addition, LST is dependent on emissivity and atmospheric effect, although the scattering effect on NIR-SWIR_{index} is significantly lower than in Visible bands. Finally, the applicability over native vegetation (e.g., native grassland) with an expectable resilience to water deficit should be analyzed in future studies.

3.3. The TIDI Sensitivity with Soil Moisture

After the calculation of daily TIDI images, a point comparison between subsurface soil moisture and the index was carried out to evaluate the sensitivity of the method to fluctuations in water availability for vegetation growth. The use of extreme LST_{max} and LST_{min} to obtain TIDI and then to analyze data in different stations was considered, given that these edges would reflect the extreme water availability of the area and period studied. Figure 10 shows the temporal evolution of TIDI and rainfall during the analyzed period. The index is sensitive to hydric conditions, decreasing after rain events (e.g., DOY 50–60 for both stations). The first days of the analyzed period (DOY 1–20) were characterized by high values of the index. Although one rainfall event occurred (44 mm in La Ydalina and 28 mm in Tandil), the index showed insignificant changes, which would suggest that such an event was not enough to increase the water content in the soil profile, especially in the summer. In both stations, the minimum soil moisture was registered on these days (e.g., La Ydalina \approx 8.1–12.0% at 60 cm depth, Tandil \approx 15.1–16.2% at 20–40 cm depth).

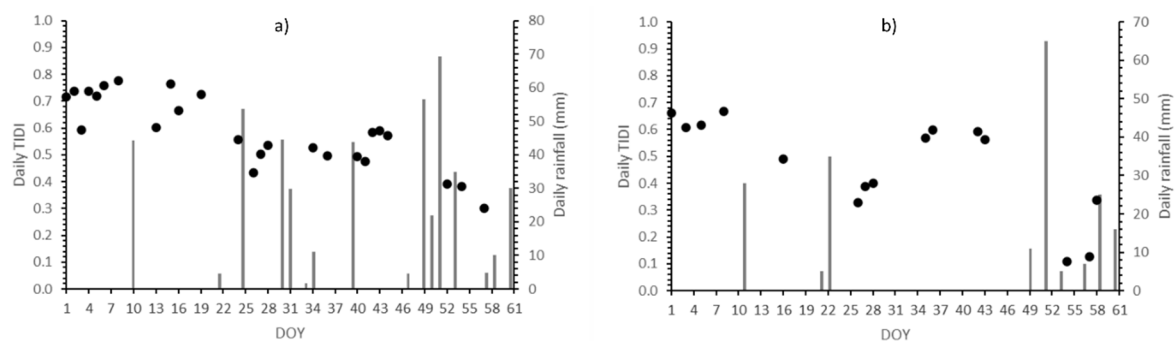


Figure 10. Daily TIDI as a function of time for (a) La Ydalina and (b) Tandil stations during the analyzed period.

The comparison with soil moisture was conducted considering values of a 3×3 kernel size centered on La Ydalina and Tandil stations. Although the relationship between optical/thermal and root-zone soil moisture is dependent on the vegetation types and climate zones, a strong negative trend was observed in both stations, with high values of the index according to low water availability in the root zone (Figure 11). These results are consistent with the process of water absorption, evapotranspiration, and changes in optical/thermal variables of plants ([26,47]. Also, they are in agreement with several studies that showed the correlation between vegetation indices and root zone soil moisture (e.g., [48–50]). Ref. [34] proposed a linear model for surface soil moisture estimation based on SWIR bands. They reported, under well-controlled laboratory conditions, the greatest sensitivity around $2.21 \mu\text{m}$ on different bare soil types. However, as these authors stated, optical methods have shallow penetration depths, as well as limited direct applicability in vegetated soils. Later, [33] suggested a model based on a linear physical relationship between soil moisture and NDVI/SWIR reflectance. They parameterized the model considering the pixel distribution within the SWIR/NDVI space, assuming linear dry and wet edges. Also, they assumed a linear relationship between soil- and vegetation-water contents and then the correlation of SWIR/NDVI with root zone soil moisture. However, experimental evidence of that is scarce and, although they showed volumetric moisture content estimation errors below $0.05 \text{ cm}^3 \text{ cm}^{-3}$, they referred to 0–5 cm depth.

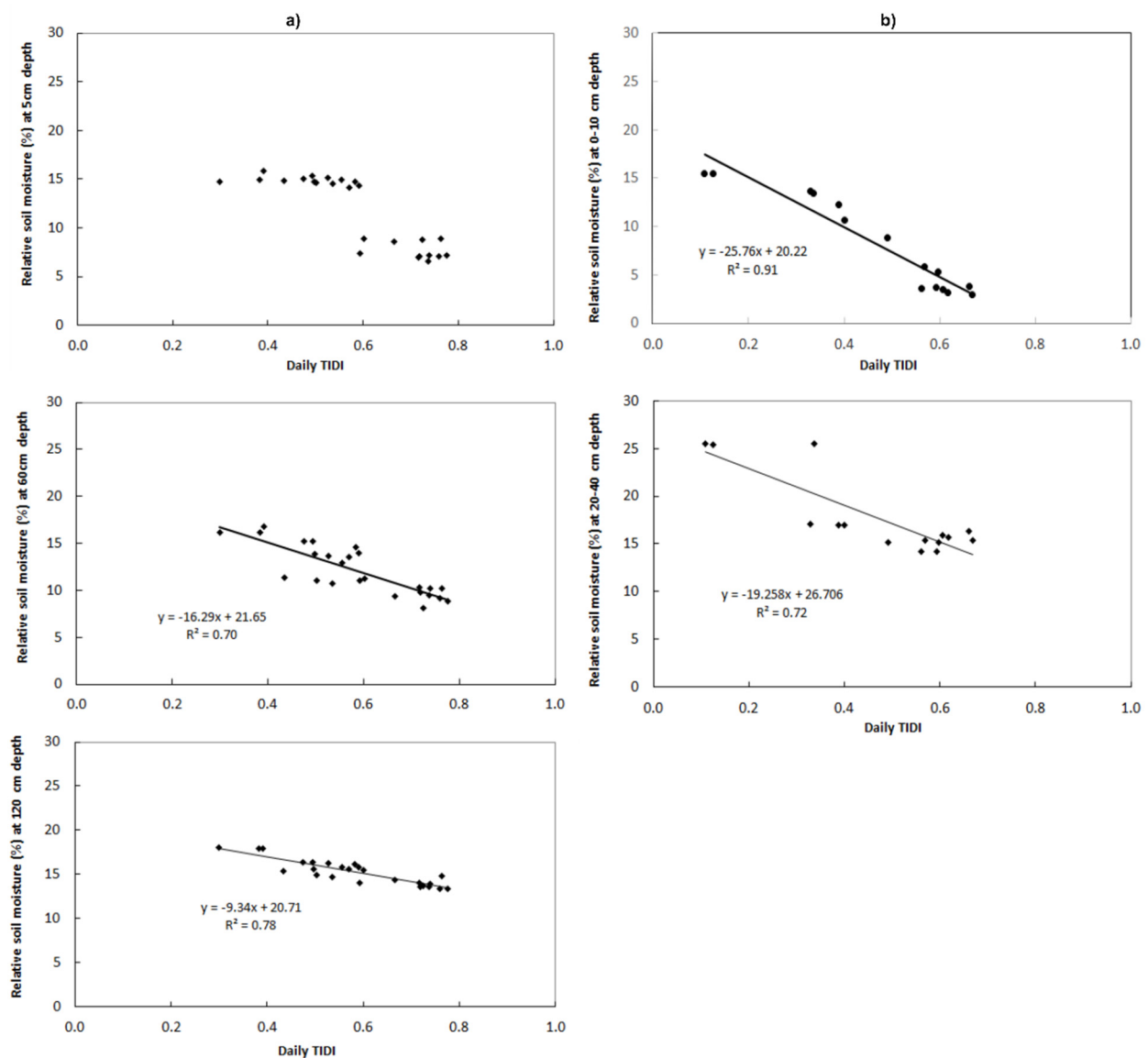


Figure 11. Relationship between daily TIDI and subsurface soil moisture in (a) La Ydalina station (N = 25, soil: Entic Hapludoll, sandy loam texture, depths of soil moisture measurements: 5 cm, 60 cm, 120 cm) and (b) Tandil station (N = 15, soil: Typic Argiudoll, silty loam texture in shallow horizons and silty clay texture in deeper horizons, depths of soil moisture measurements: 0–10 cm, 20–40 cm).

Although in our study measurements were taken at different depths, there was a trend to lower water content in the soil profile and higher index in sandy loam soils of La Ydalina (TIDI \approx 0.3–0.8) than Tandil (\approx 0.1–0.7) station (Typic Argiudoll, and silty loam texture). The former is also characterized by low organic matter content (2–3% in the A horizon vs. 3–5% in Tandil) and poorly structured soils [51]. The correlation between the index and subsurface soil moisture also depends on the structure and depth of the root system and physical limitations for root development like soil resistance to penetration ([52,53]. This would explain the correlation in deeper horizons in La Ydalina. Inversely, in Tandil, where no correlation at 60 cm depth was observed (not shown), a strong Bt horizon exists at 40 cm depth which would be a soil physical limitation producing shallow soil exploration by roots. In La Ydalina, data at 5 cm depth were included to show the behavior of surface soil moisture. Although a high R² can be obtained, two groups of points with high and low soil moisture would be producing such a correlation. Low correlation with surface data should be expected in soils with poor vertical integration (e.g., coarse texture, poor vegetation cover, and high atmospheric water demand), given the frequent

decoupling between surface and deep horizons. For example, [54] reported that the LST of a vegetated area is less responsive to surface soil moisture than the LST of bare soil because plants can extract deep water to maintain transpiration. Ref. [32] found NIR-SWIR/LST scatterplots consistent with hydric conditions in Spain. They used these data from MODIS for resampling of SMOS images, showing a high correlation with soil moisture at 0–5 cm depth. However, the association of NIR-SWIR/LST with sub-surface soil moisture deserves more attention. Although more studies should be done to evaluate the performance of NIR-SWIR/LST methods over different vegetation covers, the inclusion of NIR and SWIR to thermal data could be a complement or advance for remote monitoring of vegetation water stress in relation to traditional VI/LST methods (e.g., [25–27,55,56]).

4. Conclusions

Given the impact of water vegetation status in several plant-soil-atmosphere processes, the development of remotely sensed methods to estimate water availability for plant use is crucial. In this study, the integration of in situ and remotely sensed data of NIR and SWIR reflectance as an indicator of vegetation water content to thermal data as a proxy of energy balance changes was carried out. Field and laboratory measurements showed that NIR-SWIR reflectance reflects the changes in leaf water content. The relationship with thermal data was consistent with previous studies that separately analyzed vegetation water content indices and land surface temperature.

Daily NIR-SWIR_{index}/LST scatterplots from MODIS/Aqua were coherent with in situ measurements of spectra and LST. TIDI (Temperature-Infrared Dryness Index) maps were coherent with regional characteristics of the study area (e.g., increasing dry conditions and sandy soils westward, oceanic influence eastward). The preliminary comparison of this index calculated from MODIS/Aqua data with daily root zone soil moisture over cultivated areas ($R^2 > 0.7$) suggests the potential to reflect water availability for vegetation.

The TIDI can be an alternative to traditional VI/LST indices for vegetation dryness estimation. NIR-SWIR_{index} adds to thermal data information associated with early symptoms of water stress like stomatal conductance, while vegetation indices that consider NIR and Visible show photosynthetic damage produced by advanced water stress. Thus, indices like NDVI or EVI are conservative indicators of water deficit [28]. It should also be noted that the scattering produced by the atmosphere is significantly lower in SWIR than in Visible and NIR; therefore, its use is encouraged. The application of the method is recommended for large vegetated areas, which should have heterogeneous soil water availability for a good definition of the NIR-SWIR_{index}/LST space. Although the parameters of the index are characteristic of a heterogeneous study area with uniform atmospheric forcing, their estimation is simple. The parameterization of the model for a specific region would allow the use of this method over other croplands. The results obtained are promising, showing that the most dynamic LST fluctuations associated with the evapotranspiration process should be a complement to previous NIR-SWIR indices of the vegetation water content for comprehensive monitoring of the soil-plant system. In future studies, a full validation on different vegetation covers can be analyzed to evaluate the performance of the method for the whole estimation of the soil-plant water status. Finally, there is also a potential, not only for vegetation water stress analyses, but also in the context of hydrological and climate modeling as an input of water availability. This might play a more important role in the context of climate change, in which extreme conditions of soil moisture can be expected.

Author Contributions: Conceptualization, M.E.H. and R.E.R.; methodology, M.E.H., R.E.R. and M.I.B.; software, M.I.B.; validation, M.E.H. and M.I.B.; formal analysis, M.E.H.; investigation, M.E.H.; writing—original draft preparation, M.E.H.; writing—review and editing, M.E.H. and R.E.R.; visualization, M.E.H.; supervision, R.E.R.; project administration, R.E.R.; funding acquisition, R.E.R. and M.E.H. All authors have read and agreed to the published version of the manuscript.

Funding: This research received no external funding.

Institutional Review Board Statement: Not applicable.

Informed Consent Statement: Not applicable.

Data Availability Statement: Satellite images were downloaded from <https://search.earthdata.nasa.gov/>, accessed on 20 June 2021. Complementary field and laboratory data can be accessed at Holzman, M.; Rivas, R.; Bayala, M.; Pasapera, J. Measuring land surface temperature, near-infrared and short-wave infrared reflectance for estimation of water availability in vegetation. *MethodsX* 2021, 8, 101172, doi:10.1016/j.mex.2020.101172 or <https://data.mendeley.com/datasets/5hjy6z436/1>, accessed on 20 June 2021.

Acknowledgments: This study was supported by CONICET (Consejo Nacional de Investigaciones Científicas y Técnicas) and IHLLA (Instituto de Hidrología de Llanuras “Eduardo J. Usunoff”). The authors also would like to thank CIC (Comisión de Investigaciones Científicas de Buenos Aires), UNCPBA (Universidad Nacional del Centro de la provincia de Buenos Aires), Oficina de Riesgo Agropecuario. Also, we really appreciate the contribution of the reviewers that have helped us to improve the manuscript.

Conflicts of Interest: The authors declare no conflict of interest.

References

- Bolton, D.K.; Friedl, M.A. Forecasting crop yield using remotely sensed vegetation indices and crop phenology metrics. *Agric. For. Meteorol.* **2013**, *173*, 74–84. [[CrossRef](#)]
- Pasqualotto, N.; Delegido, J.; Van Wittenberghe, S.; Verrelst, J.; Rivera, J.P.; Moreno, J. Retrieval of canopy water content of different crop types with two new hyperspectral indices: Water absorption area index and depth water index. *Int. J. Appl. Earth Obs. Geoinf.* **2018**, *67*, 69–78. [[CrossRef](#)]
- Zhang, C.; Liu, J.; Shang, J.; Cai, H. Capability of crop water content for revealing variability of winter wheat grain yield and soil moisture under limited irrigation. *Sci. Total Environ.* **2018**, 631–632, 677–687. [[CrossRef](#)]
- Roberto, C.; Lorenzo, B.; Michele, M.; Micol, R.; Cinzia, P. Optical remote sensing of vegetation water content. In *Remote Sensing of Vegetation. Hyperspectral Indices and Image Classifications for Agriculture and Vegetation*; Thenkabail, P.S., Lyon, J.G., Huete, A., Eds.; CRC Press: Boca Raton, FL, USA, 2018; pp. 183–200. ISBN 9781138066038.
- Fensholt, R.; Huber, S.; Proud, S.R.; Mbow, C. Detecting canopy water status using Shortwave Infrared reflectance data from polar orbiting and geostationary platforms. *IEEE J. Sel. Top. Appl. Earth Obs. Remote Sens.* **2010**, *3*, 271–285. [[CrossRef](#)]
- Levitt, J. *Responses of Plants to Environmental Stresses*; Academic Press: New York, NY, USA, 1980.
- O’Toole, J.; Cruz, R. Response of leaf water potential, stomatal resistance and leaf rolling to water stress. *Plant Physiol.* **1980**, *65*, 428–432. [[CrossRef](#)] [[PubMed](#)]
- Chen, D.; Huang, J.; Jackson, T.J. Vegetation water content estimation for corn and soybeans using spectral indices derived from MODIS Near- and Short-Wave Infrared bands. *Remote Sens. Environ.* **2005**, *98*, 225–236. [[CrossRef](#)]
- Jackson, T.J.; Chen, D.; Cosh, M.; Li, F.; Anderson, M.; Walthall, C.; Doriaswamy, P.; Hunt, E.R. Vegetation water content mapping using Landsat data derived Normalized Difference Water Index for corn and soybeans. *Remote Sens. Environ.* **2004**, *92*, 475–482. [[CrossRef](#)]
- Anderson, M.C.; Neale, C.M.U.; Li, F.; Norman, J.M.; Kustas, W.P.; Jayanthi, H.; Chavez, J. Upscaling ground observations of vegetation water content, canopy height, and Leaf Area Index during SMEX02 using aircraft and Landsat imagery. *Remote Sens. Environ.* **2004**, *92*, 447–464. [[CrossRef](#)]
- Yilmaz, M.T.; Hunt, E.R.; Goins, L.D.; Ustin, S.L.; Vanderbilt, V.C.; Jackson, T.J. Vegetation water content during SMEX04 from ground data and Landsat 5 Thematic Mapper imagery. *Remote Sens. Environ.* **2008**, *112*, 350–362. [[CrossRef](#)]
- Rhee, J.; Im, J.; Carbone, G.J. Monitoring agricultural drought for arid and humid regions using multi-sensor remote sensing data. *Remote Sens. Environ.* **2010**, *114*, 2875–2887. [[CrossRef](#)]
- Ullah, S.; Skidmore, A.K.; Ramoelo, A.; Groen, T.A.; Naeem, M.; Ali, A. Retrieval of leaf water content spanning the Visible to Thermal Infrared spectra. *ISPRS J. Photogramm. Remote Sens.* **2014**, *93*, 56–64. [[CrossRef](#)]
- Datt, B. Remote sensing of water content in eucalyptus leaves. *Aust. J. Bot.* **1999**, *47*, 909–923. [[CrossRef](#)]
- Ceccato, P.; Gobron, N.; Flasse, S.; Pinty, B.; Tarantola, S. Designing a spectral index to estimate vegetation water content from remote sensing data: Part 2. Validation and Applications. *Remote Sens. Environ.* **2002**, *82*, 198–207. [[CrossRef](#)]
- Ghulam, A.; Li, Z.L.; Qin, Q.; Yimit, H.; Wang, J. Estimating crop water stress with ETM+ NIR and SWIR data. *Agric. For. Meteorol.* **2008**, *148*, 1679–1695. [[CrossRef](#)]
- Ceccato, P.; Flasse, S.; Tarantola, S.; Jacquemoud, S.; Grégoire, J.M. Detecting vegetation leaf water content using reflectance in the optical domain. *Remote Sens. Environ.* **2001**, *77*, 22–33. [[CrossRef](#)]
- Fensholt, R.; Sandholt, I. Derivation of a Shortwave Infrared Water Stress Index from MODIS Near- and Shortwave Infrared data in a Semiarid Environment. *Remote Sens. Environ.* **2003**, *87*, 111–121. [[CrossRef](#)]
- Ceccato, P.; Gobron, N.; Flasse, S.; Pinty, B.; Tarantola, S. Designing a spectral index to estimate vegetation water content from remote sensing data: Part 1: Theoretical Approach. *Remote Sens. Environ.* **2002**, *82*, 188–197. [[CrossRef](#)]

20. Bowyer, P.; Danson, F.M. Sensitivity of spectral reflectance to variation in live fuel moisture content at leaf and canopy Level. *Remote Sens. Environ.* **2004**, *92*, 297–308. [[CrossRef](#)]
21. Danson, F.M.; Bowyer, P. Estimating live fuel moisture content from remotely sensed reflectance. *Remote Sens. Environ.* **2004**, *92*, 309–321. [[CrossRef](#)]
22. Kramer, P.J.; Boyer, J.S. *Water Relations of Plants and Soils*; Academic Press: San Diego, CA, USA, 1995; ISBN 0124250602.
23. Chaves, M.M.; Pereira, J.S.; Maroco, J.; Rodriguez, M.L.; Ricardo, C.P.P.; Osório, M.L.; Carvalho, I.; Faria, T.; Pinheiro, C. How plants cope with water stress in the field. Photosynthesis and Growth. *Ann. Bot.* **2002**, *89*, 907–916. [[CrossRef](#)]
24. Porporato, A.; Laio, F.; Ridol, L.; Rodriguez-iturbe, I. Plants in water-controlled ecosystems: Active role in hydrologic processes and response to water stress III. Vegetation water stress. *Adv. Water Resour.* **2001**, *24*, 725–744. [[CrossRef](#)]
25. Holzman, M.E.; Carmona, F.; Rivas, R.; Niclòs, R. Early assessment of crop yield from remotely sensed water stress and solar radiation data. *ISPRS J. Photogramm. Remote Sens.* **2018**, *145*, 297–308. [[CrossRef](#)]
26. Holzman, M.E.; Rivas, R.; Bayala, M. Subsurface soil moisture estimation by VI-LST method. *IEEE Geosci. Remote Sens. Lett.* **2014**, *11*, 1951–1955. [[CrossRef](#)]
27. Nutini, F.; Stroppiana, D.; Busetto, L.; Bellingeri, D.; Corbari, C.; Mancini, M.; Zini, E.; Brivio, P.A.; Boschetti, M. A weekly indicator of surface moisture status from satellite data for operational monitoring of crop conditions. *Sensors* **2017**, *17*, 1338. [[CrossRef](#)]
28. Holzman, M.E.; Rivas, R.; Piccolo, M.C. Estimating soil moisture and the relationship with crop yield using surface temperature and vegetation index. *Int. J. Appl. Earth Obs. Geoinf.* **2014**, *28*, 181–192. [[CrossRef](#)]
29. Holzman, M.E.; Rivas, R. Early maize yield forecasting from remotely sensed temperature/vegetation index measurements. *IEEE J. Sel. Top. Appl. Earth Obs. Remote Sens.* **2016**, *9*, 507–519. [[CrossRef](#)]
30. Fabre, S.; Lesaignoux, A.; Olioso, A.; Briottet, X. Influence of water content on spectral reflectance of leaves in the 3–15 μm Domain. *IEEE Geosci. Remote Sens. Lett.* **2011**, *8*, 143–147. [[CrossRef](#)]
31. Buitrago, M.F.; Groen, T.A.; Hecker, C.A.; Skidmore, A.K. Changes in Thermal Infrared spectra of plants caused by temperature and water stress. *ISPRS J. Photogramm. Remote Sens.* **2016**, *111*, 22–31. [[CrossRef](#)]
32. Sánchez-Ruiz, S.; Piles, M.; Sánchez, N.; Martínez-fernández, J.; Vall-llossera, M. Combining SMOS with Visible and near/Shortwave/Thermal Infrared satellite data for high resolution soil moisture estimates. *J. Hydrol.* **2014**, *516*, 273–283. [[CrossRef](#)]
33. Sadeghi, M.; Babaeian, E.; Tuller, M.; Jones, S.B. The optical trapezoid model: A novel approach to remote sensing of soil moisture applied to Sentinel-2 and Landsat-8 observations. *Remote Sens. Environ.* **2017**, *198*, 52–68. [[CrossRef](#)]
34. Sadeghi, M.; Jones, S.B.; Philpot, W.D. A linear physically-based model for remote sensing of soil moisture using Short Wave Infrared bands. *Remote Sens. Environ.* **2015**, *164*, 66–76. [[CrossRef](#)]
35. Holzman, M.; Rivas, R.; Bayala, M.; Pasapera, J. Measuring land surface temperature, near-infrared and short-wave infrared reflectance for estimation of water availability in vegetation. *MethodsX* **2021**, *8*, 101172. [[CrossRef](#)]
36. Holzman, M.; Rivas, R.; Carmona, F.; Niclòs, R. A method for soil moisture probes calibration and validation of satellite estimates. *MethodsX* **2017**, *4*, 243–249. [[CrossRef](#)]
37. Niclos, R.; Rivas, R.; Garcia-Santos, V.; Dona, C.; Valor, E.; Holzman, M.; Bayala, M.; Carmona, F.; Ocampo, D.; Soldano, A.; et al. SMOS Level-2 soil moisture product evaluation in rain-fed croplands of the pampean region of Argentina. *IEEE Trans. Geosci. Remote Sens.* **2016**, *54*, 499–512. [[CrossRef](#)]
38. Gao, B.C.; Goetz, A.F.H. Retrieval of equivalent water thickness and information related to biochemical components of vegetation canopies from AVIRIS data. *Remote Sens. Environ.* **1994**, *4*, 155–162. [[CrossRef](#)]
39. Larcher, W. *Physiological Plant Ecology: Ecophysiology and Stress Physiology of Functional Groups*; Springer Science & Business Media: Berlin, Germany, 2003; ISBN 9783540435167.
40. Tian, J.; Philpot, W.D. Spectral reflectance features with varied soil properties during drying process. In Proceedings of the 2016 IEEE International Geoscience and Remote Sensing Symposium (IGARSS), Beijing, China, 10–15 July 2016; pp. 3106–3109. [[CrossRef](#)]
41. Tian, J.; Philpot, W. Spectral transmittance of a translucent sand sample with directional illumination. *IEEE Trans. Geosci. Remote Sens.* **2018**, *56*, 4307–4317. [[CrossRef](#)]
42. Bayala, M.I.; Rivas, R.E. Enhanced sharpening procedures on edge difference and water stress index basis over heterogeneous landscape of sub-humid region. *Egypt. J. Remote Sens. Sp. Sci.* **2014**, *17*, 17–27. [[CrossRef](#)]
43. Galvao, L.S.; Neves Epiphanyo, J.C.; Breuning, F.M.; Formaggio, A.R. Crop type discrimination using hyperspectral data. In *Hyperspectral Remote Sensing of Vegetation*; Thenkabail, P.S., Lyon, J.G., Huete, A., Eds.; CRC Press: Boca Raton, FL, USA, 2012; pp. 397–422.
44. Wang, L.; Qu, J.J.; Xiong, X.; Hao, X.; Member, S.; Xie, Y.; Che, N. A new method for retrieving band 6 of Aqua MODIS. *IEEE Geosci. Remote Sens. Lett.* **2006**, *3*, 1–5. [[CrossRef](#)]
45. Bohn, V.; Rivas, R.; Varni, M.; Piccolo, C. Using SPEI in predicting water table dynamics in Argentinian plains. *Environ. Earth Sci. J.* **2020**, *79*, 1–16. [[CrossRef](#)]
46. Ares, M.G.; Holzman, M.; Entraigas, I.; Varni, M.; Fajardo, L.; Vercelli, N. Surface moisture area during rainfall–runoff events to understand the hydrological dynamics of a basin in a plain region. *Hydrol. Process.* **2018**, *32*, 1351–1362. [[CrossRef](#)]

47. Chang, T.-Y.; Wang, Y.-C.; Feng, C.-C.; Ziegler, A.D.; Giambelluca, T.W.; Liou, Y.-A. Estimation of root zone soil moisture using apparent thermal inertia with MODIS imagery over a tropical catchment in Northern Thailand. *IEEE J. Sel. Top. Appl. Earth Obs. Remote Sens.* **2012**, *5*, 752–761. [[CrossRef](#)]
48. Liu, S.; Roberts, D.A.; Chadwick, O.A.; Still, C.J. Spectral responses to plant available soil moisture in a Californian grassland. *Int. J. Appl. Earth Obs. Geoinf.* **2012**, *19*, 31–44. [[CrossRef](#)]
49. Santos, W.J.R.; Silva, B.M.; Oliveira, G.S.; Volpato, M.M.L.; Lima, J.M.; Curi, N.; Marques, J.J. Soil moisture in the root zone and its relation to plant vigor assessed by remote sensing at management scale. *Geoderma* **2014**, *221–222*, 91–95. [[CrossRef](#)]
50. Wang, X.; Xie, H. Different responses of MODIS-derived NDVI to root-zone soil moisture in semi-arid and humid regions. *J. Hydrol.* **2007**, *340*, 12–24. [[CrossRef](#)]
51. Ares, M.G.; Bongiorno, F.; Holzman, M.; Chagas, C.; Varni, M.; Entraigas, I. Water erosion and connectivity analysis during a year with high precipitations in a watershed of Argentina. *Hydrol. Res.* **2016**, *47*, 1239–1252. [[CrossRef](#)]
52. Brady, N.C.; Weil, R.R. Soil architecture and physical properties. In *The Nature and Properties of Soils*; Englewood, C., Ed.; Prentice-Hall: Hoboken, NJ, USA, 2008; pp. 148–157.
53. Whiteley, G.M.; Dexter, A.R. Elastic response of the roots of field crops. *Physiol. Plant.* **1981**, *51*, 407–417. [[CrossRef](#)]
54. Sun, H. Two-Stage trapezoid: A new interpretation of the land surface temperature and fractional vegetation coverage space. *IEEE J. Sel. Top. Appl. Earth Obs. Remote Sens.* **2016**, *9*, 336–346. [[CrossRef](#)]
55. Mallick, K.; Bhattacharya, B.K.; Patel, N.K. Estimating volumetric surface moisture content for cropped soils using a soil wetness index based on surface temperature and NDVI. *Agric. For. Meteorol.* **2009**, *149*, 1327–1342. [[CrossRef](#)]
56. Sandholt, I.; Rasmussen, K.; Andersen, J. A simple interpretation of the surface Temperature/Vegetation Index space for the assessment of surface moisture stress. *Remote Sens. Environ.* **2002**, *79*, 213–224. [[CrossRef](#)]